



Eidgenössische Technische Hochschule Zürich  
Swiss Federal Institute of Technology Zurich

# Simulations of CPHASE Gate Adiabaticity

Semester Thesis

Manish Jung Thapa

April 14th, 2016

Supervisor: MSc. Johannes Heinsoo

Group leader: Prof. Andreas Wallraff

Group: Quantum Device Lab, ETH Zürich

---

## Abstract

In this thesis, time-dependent hamiltonian is simulated for CPHASE gate to investigate its dependence to the gate adiabaticity parameter. The CPHASE gate is implemented with the help of two superconducting transmon type qubits. Interaction between  $|11\rangle$  and  $|20\rangle$  states is exploited to implement this gate. Rectangular magnetic flux pulse sent to one of the qubit frequency bias is used to tune these two states to resonance. For fast enough pulse rise time, the frequency of qubit is shifted non-adiabatically to achieve the desired CPHASE gate operation. For practical reasons, the flux pulse is gaussian-convoluted. The width  $\sigma$  of the gaussian characterizes the adiabaticity parameter of the gate. Maximum attainable fidelity is estimated for different  $\sigma$ . The results in this thesis show that even at finite pulse rise times, good fidelities are achieved. For  $\sigma$  of 1.78 ns, 3.57 ns, and 5.34 ns, it is shown that fidelities above 99.9% is merely attainable. These adiabaticity parameters correspond to the gate times of 61.9 ns, 66 ns and 72 ns respectively, for coupling strength between  $|11\rangle$  and  $|20\rangle$  of 8.33 MHz. Geometric phase of  $180^\circ$  is observed for all the investigated adiabaticity parameters. In addition, non-adiabatic error is seen at strong non-adiabatic regimes. In this regime, owing to the steep rise time of the flux pulse, some of the population is lost to other states.

---

# Contents

---

<b>Contents</b>	<b>ii</b>
<b>1 Introduction</b>	<b>1</b>
1.1 Motivation . . . . .	1
1.2 Quantum gates . . . . .	2
1.2.1 Single-qubit gates . . . . .	3
1.2.2 Two-qubit gates . . . . .	3
<b>2 Quantum computing with superconducting circuits</b>	<b>5</b>
2.1 Electric harmonic oscillator . . . . .	5
2.2 The cooper-pair box qubit . . . . .	6
<b>3 CPHASE gate implementation</b>	<b>10</b>
3.1 Geometric phase . . . . .	10
3.2 Time dependent qubit detuning . . . . .	12
3.3 Simulating the propagator with Dyson series . . . . .	12
3.4 Identifying the gate parameters . . . . .	14
3.5 Investigating the gate adiabaticity . . . . .	17
3.6 Experimental results . . . . .	18
<b>4 Non-adiabatic error</b>	<b>21</b>
<b>5 Conclusion</b>	<b>23</b>
<b>A Appendix</b>	<b>25</b>
A.1 Simulation results in non-adiabatic regime . . . . .	25
A.2 Wolfram Mathematica framework for simulations . . . . .	26
<b>Bibliography</b>	<b>27</b>

## Introduction

---

The basic unit of quantum information is called qubit. Unlike bits in classical computers, qubits can be in both state  $|0\rangle$  and  $|1\rangle$  at the same time. Two qubits can be in states  $|00\rangle$ ,  $|01\rangle$ ,  $|10\rangle$  and  $|11\rangle$  at the same time. For each additional qubits, the total number of states doubles. Although such states cannot be measured directly, it is the natural existence of these kinds of states that give quantum computers their ability to process large amounts of data quicker than any classical computers. Quantum computers hold remarkable promises to speed up one's computational task on day-to-day basis. It promises to aid researchers to solve complex problems like simulations of large biological molecules or factoring large numbers using Shor's algorithm. In addition, blue print for provably secure cryptography techniques exists that is only possible within the realm of quantum computers. The following sections briefly describe the fundamental elements of quantum computing, especially the idea universal quantum gates.

### 1.1 Motivation

Quantum computing mainly involves three steps for qubits: initialization, unitary evolution and readout. Manipulation of qubits defines the unitary evolution of quantum information. Classical computers are built of electrical circuits, and it involves logic gates to manipulate the classical bits. In quantum computers, qubit states are manipulated with the help of quantum gates. Several quantum gates are applied in sequence to accomplish the desired unitary evolution of the qubit states. However, there are several possible unitary operators. Constructing a special gate for each of the operations we would like to perform on our qubit state is time-consuming. This is where the idea of universal set of quantum gates comes in handy. Universal set of gates act as building blocks for other gates, and more complex gates can be constructed using the elements from just this set. It is

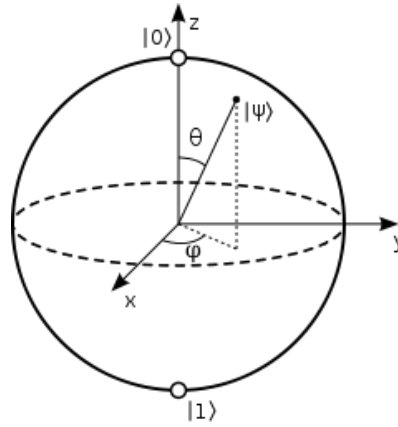


Figure 1.1: A geometrical display of two-level quantum system.

easy to see from our basic quantum information processing lecture that the gates CNOT, Hadamard  $H$  and Phase  $T$  gate make up the universal set of quantum gates. Furthermore, CNOT gate is equivalent to CPHASE gate up to local unitary operations. This is why CPHASE gate is a very useful two-qubit gate in quantum computing. In the section below, the circuit diagram and operation principle of some of the important single-qubit and two-qubit gates are shown. To know more about the universal set of quantum gate, I would like to refer readers to the textbook (Nielsen and Chuang, 2000).

## 1.2 Quantum gates

A qubit state is described by a vector  $|\psi\rangle = a|0\rangle + b|1\rangle$ , where  $a$  and  $b$  are complex or real numbers such that  $|a|^2 + |b|^2 = 1$ . In classical computing, the state of a bit can be determined with 100 % accuracy to be in state  $|0\rangle$  or  $|1\rangle$ . However, in quantum computing, the measurement of qubit in standard basis will "force" the qubit to be in state  $|0\rangle$  or  $|1\rangle$  with probabilities  $|a|^2$  and  $|b|^2$ , respectively. This observation lies at the heart of quantum mechanics, and famously comes from the Copenhagen interpretation of quantum mechanics devised in the mid 1920s. The state of the qubit can be understood better geometrically as shown in Figure 1.1. Qubit state can be written in the following manner:

$$|\psi\rangle = \cos\frac{\theta}{2}|0\rangle + e^{i\varphi}\sin\frac{\theta}{2}|1\rangle \quad (1.1)$$

where  $\theta$  and  $\varphi$  are real numbers. The parameters  $\theta$  and  $\varphi$  define a point  $(\sin\theta\cos\varphi, \sin\theta\sin\varphi, \cos\theta)$  on the surface of a Bloch sphere (Nielsen and Chuang, 2000).

### 1.2.1 Single-qubit gates

Unitary operation on single qubit state is a rotation on the surface of a Bloch sphere. The set  $[\hat{H}, \hat{T}]$  can be used to construct arbitrary single-qubit gates. The following shows the matrix representation of  $\hat{H}$  and  $\hat{T}$ :

$$\hat{H} = \frac{1}{\sqrt{2}} \begin{bmatrix} 1 & 1 \\ 1 & -1 \end{bmatrix} \quad (1.2)$$

$$\hat{T} = \begin{bmatrix} 1 & 0 \\ 0 & e^{i\pi/4} \end{bmatrix} \quad (1.3)$$

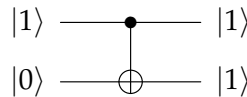
Take for instance the following sequence of operation involving  $\hat{H}$  and  $\hat{T}$ :

$$\begin{aligned} \hat{U} &= \hat{T}\hat{H}\hat{T}\hat{H} = e^{-i\pi/8\hat{\sigma}_z} e^{-i\pi/8\hat{\sigma}_x} \\ &= \cos^2\frac{\pi}{8}I - i\sin\frac{\pi}{8}[\cos\frac{\pi}{8}(\hat{\sigma}_x + \hat{\sigma}_z) + \sin\frac{\pi}{8}\hat{\sigma}_y] \end{aligned} \quad (1.4)$$

here  $\hat{U}$  describes rotation about the axes  $\vec{n}=(\cos\frac{\pi}{8}, \sin\frac{\pi}{8}, \cos\frac{\pi}{8})$  by an angle  $\theta$  such that  $\cos\frac{\theta}{2} = \cos^2\frac{\pi}{8}$ . When  $\hat{U}$  is sandwiched between two  $\hat{H}$  operators, the new unitary describes rotation around another axis  $\vec{m}=(\cos\frac{\pi}{8}, -\sin\frac{\pi}{8}, \cos\frac{\pi}{8})$  such that  $|\vec{m}\cdot\vec{n}| < 1$ . Multiple use of  $\hat{H}$  and  $\hat{T}$  accomplishes rotation around two-non parallel axes  $\vec{m}$  and  $\vec{n}$  (Nielsen and Chuang, 2000). The next section describes another element of universal quantum gates which is conditional two-qubit gates.

### 1.2.2 Two-qubit gates

Two-qubit control operations are necessary in both classical and quantum computing. One of the very basic control operations in quantum computing is CNOT gate (where C stands for conditional). This gate consists of two parts: control qubit and target qubit. In this gate, operation is turned on or off depending on the state of the control qubit. For instance, if the control qubit is excited, the operation flips the state of target qubit; if the control qubit is not excited, the operation does nothing to the target qubit. The circuit diagram and matrix representation in the computational basis for CNOT gate is given below:



$$\hat{U}_{CNOT} = \begin{bmatrix} 1 & 0 & 0 & 0 \\ 0 & 1 & 0 & 0 \\ 0 & 0 & 0 & 1 \\ 0 & 0 & 1 & 0 \end{bmatrix} \quad (1.5)$$

CNOT gate along with single qubit unitaries form the elements of the universal set of quantum gates. Furthermore, this gate can be directly constructed with the help of another important two qubit gate known as CPHASE gate. CNOT gate can be constructed by applying Hadamard gate to the target qubit, CPHASE gate to this new state and Hadamard gate again (Steffen, 2013). Below shows the circuit diagram and matrix representation for the CPHASE gate:

$$\begin{array}{c}
 |1\rangle \text{ --- } \bullet \text{ --- } |1\rangle \\
 |1\rangle \text{ --- } \bullet \text{ --- } -|1\rangle
 \end{array}$$

$$\hat{U}_{CPHASE} = \begin{bmatrix} 1 & 0 & 0 & 0 \\ 0 & 1 & 0 & 0 \\ 0 & 0 & 1 & 0 \\ 0 & 0 & 0 & -1 \end{bmatrix} \quad (1.6)$$

CPHASE gate flips the phase of the two-qubit state if both the qubits are excited. Unlike CNOT gate, CPHASE gate is symmetric. By exploiting the evolution of population through the non-computational sub-system, CPHASE gate is implemented by coupling between two qubit states:  $|11\rangle$  and  $|20\rangle$  (Strauch et al., 2003). During this closed evolution cycle through  $|20\rangle$ ,  $|11\rangle$  state picks up a geometric phase of  $180^\circ$ . In addition, phases are shifted from the lab reference frame because the flux pulse causes detuning of the transition frequencies of the qubits. This additional phases qubits individually acquire is called dynamic phase, and should be compensated using single-qubit rotations. More will be discussed about the implementation of CPHASE gate in the later sections. The next section outlines basic elements of quantum computer, realized in the architecture of superconducting circuits.

## Quantum computing with superconducting circuits

---

Under certain physical conditions, macroscopic objects show quantum mechanical behavior. Superconducting electronic circuits demonstrate quantum mechanical properties if well-isolated from the environment. These circuits allow negligibly small dissipation. A superconducting circuit consists of inductor and capacitor connected by a superconducting metallic wire. This circuit functions like an artificial atom. The non-linearity in the energy levels of superconducting qubits comes by using a non-linear inductor known as Josephson junction.

### 2.1 Electric harmonic oscillator

One of the simplest quantum circuits is an LC oscillator (Devoret, 1997). The Hamiltonian of this quantum circuit can be written in the basis of  $\Phi$  and  $q$  as follows:

$$H(q, \Phi) = \frac{q^2}{2C} + \frac{\Phi^2}{2L} \quad (2.1)$$

where  $C$  is the capacitance of capacitor and  $L$  is the inductance of inductor. At this point, a parallel could be drawn with the regular harmonic oscillator consisting of momentum  $p$  and position  $x$  degrees of freedom. In superconducting LC circuit, flux  $\Phi$  behaves like canonical momentum  $p$  and charge  $q$  behaves like its conjugate  $x$ . One can use canonical quantization to write these conjugate variables in terms of quantum mechanical hermitian operators  $\hat{q}$  and  $\hat{\Phi}$ . These operators do not commute with each other, and now



the Hamiltonian can be expressed in the following manner:

$$\hat{H} = \hbar\omega(\hat{a}^\dagger\hat{a} + \frac{1}{2}) \quad (2.2)$$

where  $\omega = 1/\sqrt{LC}$  and  $a = (\hat{\Phi} + iZ\hat{q})/\sqrt{2\hbar Z}$  with  $Z = \sqrt{L/C}$ . The energy levels of the harmonic oscillator are evenly spaced. However, to make a qubit, one needs to introduce anharmonicity in the spectrum, and hence be able to isolate the two-levels from each other. This is done by introducing a non-linear inductor known as Josephson junction in the circuit (Nakamura et al., 1997). This is described in the next section.

## 2.2 The cooper-pair box qubit

A Josephson junction is an electronic device that is constructed of two superconducting electrodes with a thin insulator in between. The spectrum of superconducting oscillator described above is made non-linear by including the Josephson junction as a non-linear inductor. It is the only non-linear resonator that experiences no energy dissipation. If the distance between two superconducting electrodes is very small, the Cooper pairs present tunnel through this gap thereby producing the current  $I$ . The following equations describe the current flowing through and voltage across the Josephson junction (Tinkham, 1975):

$$I = I_0 \sin\delta \quad (2.3)$$

$$V = \frac{\Phi_0}{2\pi\delta} \quad (2.4)$$

where  $I_0$  is critical current,  $\Phi_0$  is the magnetic flux quantum and  $\delta$  signifies the phase difference between the two electrodes. Critical current is controllable, and depends on the geometry of the Josephson junction. It can be changed by changing the area of the junction. From these Josephson equations follows the following relation for voltage and current:

$$V = \frac{\Phi_0}{2\pi I_0} \frac{1}{\cos\delta} \quad (2.5)$$

Here the voltage  $V$  is clearly non-linear in phase difference  $\delta$ . In addition,  $\Phi_0/2\pi I_0$  is quantified as specific Josephson inductance  $L_{J_0}$ , and the quantity  $\Phi_0 I_0/2\pi$  is called the Josephson energy  $E_J$ . This shows time-dependent phase between two electrodes can be realized by biasing the junction with voltage. Such circuit with AC Josephson junction is referred to as the Cooper

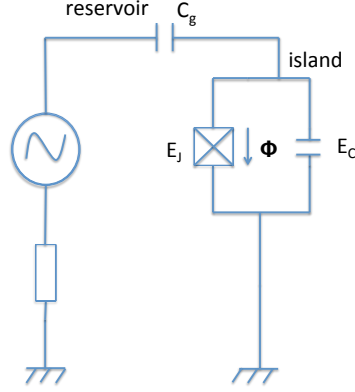


Figure 2.1: Circuit diagram of a CPB. The Cooper pairs tunnel into the reservoir from the island carrying a certain amount of current (Dewes, 2012)

pair box (CPB) (Taylor et al., 1967). As can be seen in Figure 2.1, it is formed of superconducting island which is connected by a Josephson junction to a reservoir electrode (having capacitance  $C_g$ ). The Cooper pairs can tunnel back and forth from island to the reservoir. The state of the qubit is described by the number of tunneled Cooper pairs into the reservoir.

The total electrostatic energy of CPB is given by:

$$E_{el} = (2e)^2 \frac{(N - n_g)^2}{2C_\Sigma} \quad (2.6)$$

where  $N$  is the excess Cooper pairs in island,  $n_g$  is the charge in gate capacitor,  $C_\Sigma = C_J + C_g$ ,  $C_J$  is the Josephson capacitance,  $C_g$  is the reservoir (gate) capacitance. The amount of Cooper pairs tunneling into the island can be controlled by controlling the gate voltage applied to  $C_g$ . The total magnetic energy of CPB is written as follows:

$$E_{mag} = -E_J \cos \delta. \quad (2.7)$$

When two of these Josephson junction is present in the circuit, the so-called SQUID (Superconducting Quantum Interference Device) is formed. If these junctions have same  $E_j$ , a SQUID with single effective Josephson energy  $E_j(\Phi) = 2E_j |\cos(\pi\Phi/\Phi_0)|$  can be considered. Such SQUID allows one to tune qubit frequency by influencing  $E_j(\Phi)$  by applying magnetic flux  $\Phi$ .

More of SQUID can be understood from the book (Tinkham, 1975). The Hamiltonian of CPB can then be written as follows:

$$\hat{H} = (2e)^2 \frac{(\hat{N} - n_g)^2}{2C_\Sigma} - E_J(\Phi) \cos \hat{\delta} \quad (2.8)$$

with commutation for  $\hat{N}$  and  $\hat{\delta}$  as  $[\hat{N}, \hat{\delta}] = i$ . Further  $\cos \hat{\delta}$  can be written as  $\frac{1}{2}(e^{i\hat{\delta}} + e^{-i\hat{\delta}})$ . The quantity  $e^{\pm i\hat{\delta}}$  acts as the raising and lowering operator for the number of cooper pairs on the island by one. This describes the tunneling of the cooper pairs across the Josephson junction. The Hamiltonian in Equation 2.8 can now be expanded in the following manner:

$$\hat{H} = \sum_{N=1}^{\infty} (E_c(\hat{N} - n_g)^2 |N\rangle\langle N| - \frac{E_J}{2} (|N\rangle\langle N+1| + |N+1\rangle\langle N|)). \quad (2.9)$$

Figure 2.2 can be interpreted looking at such hamiltonian in charge representation. In the absence of a Josephson coupling, the number of Cooper pairs on island is fixed at  $N$ . This is the case when only capacitor is present in the circuit. The energy then is parabolic in  $n_g$ , as can be seen from the dotted line. Turning on the Josephson energy  $E_J$  will lift the charge degeneracy occurring at  $n_g=0.5, 1.5$ , etc. leading to avoided crossing at these points. In order to find the spectrum of CPB Hamiltonian, one needs to solve the Schrodinger equation. One drawback of the hamiltonian in Equation 2.9 is that it cannot be solved analytically. To receive a spectrum of Figure 2.2, one needs to go to the phase representation of CPB hamiltonian. This hamiltonian is then exactly solvable in terms of *Mathieu functions* (Cottet, 2002). Below shows the CPB hamiltonian in phase representation:

$$E_k \psi_k(\delta) = (E_c(-i \frac{\partial}{\partial \delta} - n_g)^2 - E_J(\varphi) \cos(\delta)) \psi_k(\delta) \quad (2.10)$$

where  $\psi_k(\delta)$  is the wave function in phase basis for  $k^{th}$  excitation.

The readout of the state of superconducting qubit is done by coupling the CPB to a superconducting LC oscillator (Wallraff et al., 2004). A Jaynes-Cummings (JC) type hamiltonian can be realized in this architecture. The cavity is the superconducting LC oscillator, and atom is the Cooper pair box. Readout is done under the dispersive regime of driven JC hamiltonian.

$$\hat{H}' \approx \hbar(\omega_r + \frac{g^2}{\Delta} \hat{\sigma}_z) \hat{a}^\dagger \hat{a} + \frac{\hbar}{2} (\omega_a + \frac{g^2}{\Delta}) \hat{\sigma}_z, \quad (2.11)$$

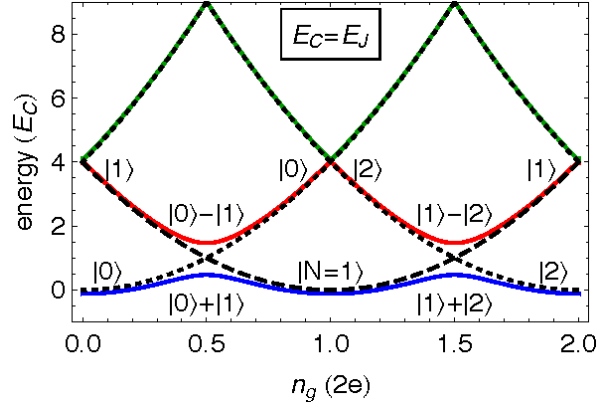


Figure 2.2: This shows the energy spectrum of CPB for excitations  $k=0,1$  and  $2$  for  $E_j = E_C$  (Baur, 2012)

where resonator-qubit coupling constant  $g = C_g/C_\Sigma 2e/\hbar\sqrt{\hbar\omega_r/2C}$ ,  $\omega_r$  is the resonator frequency,  $C_g$  is the gate capacitance and  $C$  is the resonator capacitance. Clearly in this dispersive JC regime, the weak microwave drive applied to the resonator is on resonance to it at different frequencies depending on whether qubit is at ground state or excited state. Looking at the transmission spectrum of the coherent microwave drive, readout of the CPB qubit is performed.

One important downside, though, of CPB is that it is sensitive to the surrounding charge fluctuations. This can be overcome by making the spectrum of CPB less dependent to the gate charge. This is achieved at the so-called transmon regime,  $E_j \gg E_C$ . The decrease in the charge fluctuation sensitivity of the qubit in the transmon regime comes at the cost of reduced anharmonicity. However, qubit anharmonicity decreases relatively slowly in comparison to the exponential decrease in the charge noise sensitivity of the transmon qubit. Thus, the transmon qubit still sufficiently demonstrates relatively large anharmonicity. (Koch et al., 2007).

## Chapter 3

---

# CPHASE gate implementation

---

Two-qutrits are considered in the simulation of the CPHASE gate. The hamiltonian is composed of bare  $\hat{H}_{bare}$  and interaction  $\hat{H}_{int}$  parts:

$$\hat{H} = \hat{H}_{bare} + \hat{H}_{int}. \quad (3.1)$$

The interaction Hamiltonian for the coupled qutrits looks as follows:

$$\hat{H}_{int} = J[(|0\rangle\langle 1|_A + \sqrt{2}|1\rangle\langle 2|_A) \otimes (|1\rangle\langle 0|_B + \sqrt{2}|2\rangle\langle 1|_B) + h.c]. \quad (3.2)$$

The relevant coupling term for the implementation of CPHASE gate is given below:

$$\hat{H}_{int} = J_0(|20\rangle\langle 11| + |11\rangle\langle 20|). \quad (3.3)$$

$\hat{H}_{bare}$  part of the Hamiltonian describes the two-qutrit system in the absence of exchange coupling  $J$ . Energy spectrum of this part can be tuned by sending a magnetic flux pulse through one or both of the qutrit frequency biases. At first, the qutrit frequencies are set at the so-called parking frequencies. At the parking frequency, the exchange interaction between two-qutrits is strongly suppressed. In this simulation, qutrit A is parked at 5.37 GHz with anharmonicity of 0.3 GHz, and qutrit B is parked at 4.81 GHz with anharmonicity of 0.3 GHz.  $J_0$  is about 8.33 MHz.

### 3.1 Geometric phase

One way of implementing two-qubit CPHASE gate is to tune the frequency of one of the qubit along the adiabatic trajectory that shifts  $|11\rangle$  state very close to the avoided crossing with  $|20\rangle$  state. Doing so  $|11\rangle$  state acquires

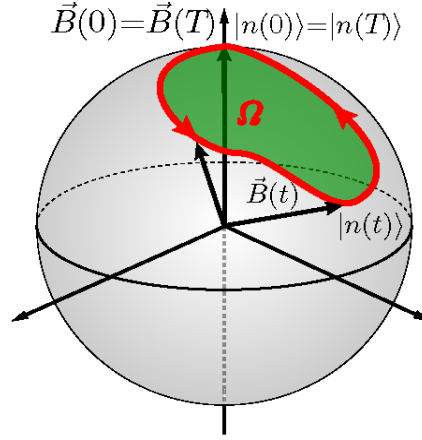


Figure 3.1: The trajectory of this quantum system is represented by a closed loop on Bloch sphere. The solid angle  $\Omega$  swept around the Bloch sphere is proportional to the geometric phase the quantum system acquires. This geometric phase is also known as Berry phase (Berry, 1984).

state-dependent relative phase shift that is dynamic in nature. The adiabatic trajectory is optimized such that as minimal population as possible leaks into the  $|20\rangle$  state, thereby giving a phase shift of  $-1$  (Martinis and Geller, 2014). A different way to implement two-qubit gates is to manipulate the evolution of quantum system geometrically. This is supposedly more robust against noise in the control parameters. If the evolution of quantum system is cyclic, the system returns to its original state picking up a geometric phase. Figure 3.1 demonstrates cyclic evolution of some quantum system on a Bloch sphere. In this example, magnetic field induces transition of the quantum system.

In this thesis, the CPHASE gate is implemented geometrically by exploiting the avoided crossing between states  $|20\rangle$  and  $|11\rangle$ . It involves exciting the quantum state non-adiabatically out of the computational sub-system and back again by applying magnetic flux pulse to one of the qubits. This closed evolution of qubits around a Bloch sphere induces geometric phase shift of  $-1$  for certain pulse parameters. A time-dependent magnetic flux pulse tunes  $|20\rangle$  and  $|11\rangle$  states to resonance, and subsequently the population of  $|11\rangle$  state undergoes oscillation. In this simulation, to tune the qubit frequency, a rectangular pulse is sent to the qubit A frequency bias through a Gaussian filter of width  $\sigma$ . This pulse introduces time-dependent detuning of qubit A, thereby bringing  $|20\rangle$  and  $|11\rangle$  to resonance. The next section briefly outlines the parameters and shape of this detuning flux pulse.

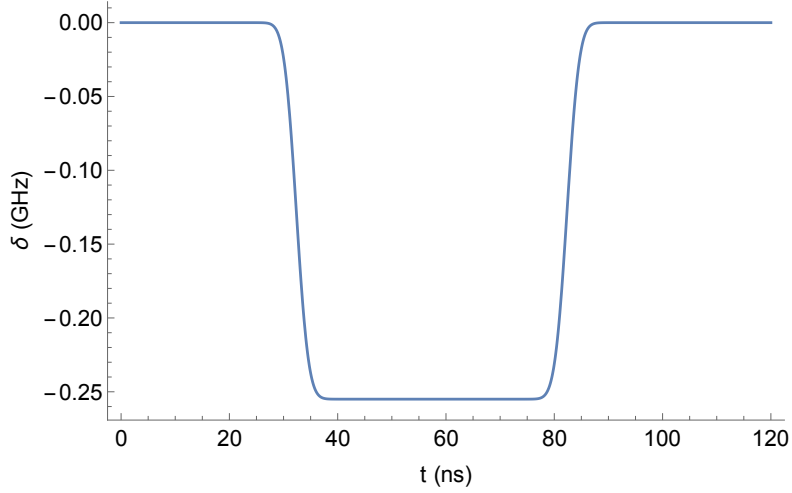


Figure 3.2: Time-dependent detuning. The interaction length is the flat region of the pulse. For infinitely non-adiabatic pulse, for interaction length of  $1/2J_0$  and resonance, a CPHASE gate is executed.

### 3.2 Time dependent qubit detuning

The pulse that detunes qutrit A consists of two parameters, qutrit detuning  $\delta$  and length  $t_{len}$ , in addition to the adiabaticity parameter. The detuning pulse profile is shown in Figure 3.2. The pulse length  $t_{len}$  is defined as the full-width at half minimum (FWHM). This pulse is constructed by convoluting a rectangular pulse with a Gaussian of a certain standard deviation  $\sigma$ .  $\sigma$  represents the adiabaticity parameter. In this simulation, the frequency of only qubit A is tuned in time with this flux pulse. The energy spectrum of two-qutrit states  $|20\rangle$  and  $|11\rangle$  are shown in Figure 3.3. To achieve the CPHASE gate operation, the pulse amplitude and length is chosen such that population evolves through a non-computational sub-system. Evolution through this closed loop leads to state  $|11\rangle$  picking up geometric phase of  $180^\circ$  for specific pulse parameters. In addition, clearly the Hamiltonian in Equation 3.1 is time-dependent because frequency of one of the qubits is changing in time. The next section presents a method to numerically solve this time-dependent Schrodinger equation using the so-called Dyson series to achieve the simulated CPHASE propagator  $\hat{U}_{sim}$ .

### 3.3 Simulating the propagator with Dyson series

As discussed above, the two-qutrit system Hamiltonian is time-dependent. Thus, to get the CPHASE propagator, one needs numerically evaluate matrix

### 3.3. Simulating the propagator with Dyson series

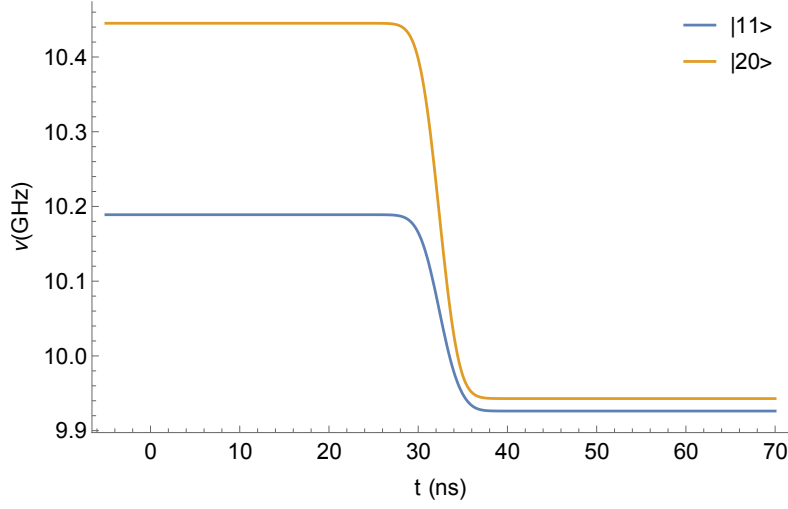


Figure 3.3: Spectrum of energy levels for  $|20\rangle$  and  $|11\rangle$  states. Only qubit A is detuned in time.

of this form:

$$\hat{U}_{sim} = e^{-\int_0^t \hat{H}(t') dt'}, \quad (3.4)$$

but clearly  $\hat{H}(t)$  do not commute at different times, and therefore

$$e^{\hat{H}(t_a)} e^{\hat{H}(t_b)} \neq e^{\hat{H}(t_a) + \hat{H}(t_b)}. \quad (3.5)$$

First the approximate solution for the propagator  $\hat{U}_{sim}$  can simply be written in the integral form:

$$\hat{U}_{sim}(t) = I - \int_0^t \hat{H}(t') \hat{U}_{sim}(t') dt'. \quad (3.6)$$

Iterating the Equation 3.6 for a fixed simulation window of  $t$  leads to the following series:

$$\begin{aligned} \hat{U}_{sim}(t) = I - i \int_0^t \hat{H}(t') dt' + (-i)^2 \int_0^t dt'' \int_0^{t'} \hat{H}(t') \hat{H}(t'') dt' + \dots \\ + (-i)^n \int_0^t dt'' \dots \int_0^{t^n} \hat{H}(t') \dots \hat{H}(t^n) dt^n. \end{aligned} \quad (3.7)$$

The series in equation 3.7 is known as the Dyson series. Here the operators are time-ordered. However, to avoid solving complicated higher dimen-



sional integrals, this series is approximated as the product of propagator at small time slices:

$$\hat{U}_{sim}(t) = \prod_{n=0}^N e^{-i\hat{H}(ndt')dt'}, \quad (3.8)$$

where  $N = t/dt' - 1$ . Practically, the simulation window  $t$  is split into smaller pieces, and the product of propagators at these smaller time pieces is evaluated. To increase the accuracy, one should use many number  $N$  of terms in the product. In the simulation of CPHASE gate, the simulation window was fixed at 180 ns, and about 750 terms in the product in Equation 3.8 was used. The results received from this approximation was compared to the built-in differential equation solver on *Wolfram Mathematica* known as *NDSolve*. The calculations for population, phase and fidelity agree up to the fourth decimal place in the worst case. Simulating CPHASE gate with Dyson series as opposed to *NDSolve* is more efficient computationally. In fact, the former is almost ten times faster as compared to the later. This is very advantageous as it makes simulation of high resolution CPHASE gate possible. Accurate identification of the pulse parameters to execute CPHASE gate is done by sweeping through several  $\delta$  and  $t_{len}$  points. The next section illustrates how to identify these pulse parameters for executing good-fidelity CPHASE gate.

### 3.4 Identifying the gate parameters

In this thesis, the simulation of CPHASE gate is focused for the Qudev lab gate scheme, which uses the adiabaticity parameter  $\sigma$  of 1.78 ns. As mentioned above, this quantity is defined as the standard deviation of the Gaussian filter. In addition, to understand if adiabaticity plays a role in the fidelity of CPHASE gate, other adiabaticities are also investigated. 2-dimensional plots are created for population, geometric phase and fidelity, sweeping through 1250 of  $\delta$  points and 140 of  $t_{len}$  points. In this thesis, fidelity of the CPHASE gate was calculated using the following definition (Pedersen, 2008):

$$F_{CPHASE} = \frac{|Tr[\hat{U}_{ideal}^\dagger \hat{U}_{sim}]|^2 + Tr[\hat{U}_{ideal}^\dagger \hat{U}_{ideal}]}{20}. \quad (3.9)$$

Here  $\hat{U}_{sim}$  refers to the propagator constructed out of hamiltonian in Equation 3.1, and  $\hat{U}_{ideal}$  refers to the ideal CPHASE gate from Equation 1.6. The above-definition of fidelity is explicitly used because in the implementation of CPHASE gate population moves through non-computational states. In addition, one needs to project  $\hat{U}_{sim}$  into the computational subspace of two

qubits to calculate the fidelities for different  $\delta$  and  $t_{len}$ . Figure 3.5 shows the fidelity landscape for  $\sigma = 1.78$  ns. Fidelity above 99.9% can be seen for this adiabaticity parameter.

To accurately estimate the optimal CPHASE gate parameters, the final population of  $|11\rangle$  state under the operation of  $\hat{U}_{sim}$  is computed for several  $\delta$  and  $t_{len}$  points. The simulated population landscape looks like the so-called Chevron pattern. As can be seen on Figure 3.4 (a), the population oscillates at the smallest frequency when  $|20\rangle$  and  $|11\rangle$  states are on resonance, at about  $\delta = -0.2555$  GHz. In addition, the fidelity contour at 99% is overlaid onto the density plot of the population. At the adiabaticity parameter  $\sigma$  of 1.78 ns, the shortest CPHASE gate length is found at about 61.9 ns. Other solutions also occur but at longer pulse length, as illustrated by other 99% fidelity contours. The population landscape also looks asymmetric about resonance. This is due to the finite rise time of flux pulse, and has been confirmed experimentally using the setup presented in the next section. Figure 3.9. shows experimental demonstration of the Chevron pattern. Qubit populations are extracted by looking at the transmission spectrum of the qubit which is coupled with the resonator. Although one should keep in mind that accurately estimating the population experimentally is limited by various factors such as inaccuracy in single-qubit rotations as well as low frequency noise in measurement instruments (Dahlberg, 2016).

Identifying the exact gate parameters with population landscape has one major downside. The Chevron pattern shows the maximum population is received back to the computational subsystem at other  $\delta$  points also. But the phase of  $180^\circ$  is only achieved for a specific  $\delta$ 's. To overcome this problem, one needs to look at the geometric phase landscape. The geometric phase  $|11\rangle$  state picks up is measured in two parts. Two Ramsey-type measurements are performed. At first, qubit B is excited while qubit A is in superposition state:  $\frac{1}{\sqrt{2}}(|0\rangle + |1\rangle) \otimes |1\rangle$ . Second, qubit B is in ground state while qubit A is in superposition state:  $\frac{1}{\sqrt{2}}(|0\rangle + |1\rangle) \otimes |0\rangle$ . Now, when qubit A is tuned to qubit B with the help of flux pulse, state-dependent geometric phase is picked up by the superposition state of the latter case. The relative phase is then measured between these two cases. This will give us the geometric phase landscape of Figure 3.4 (b). The geometric phase landscape looks tilted about resonance as some conditional dynamic phase is picked up by qubits during the pulse rise time. In addition, qubits A and B also individually pick up some dynamic phases,  $\varphi_A$  and  $\varphi_B$  respectively. The phases of two qubits are shifted from the rotating frame of parking frequencies,  $\nu_A$  and  $\nu_B$  by amount  $\varphi_{A,B} = \int_0^t (\nu_{A,B}^{parking} - \nu_{A,B}(t')) dt'$ . This shift needs to be compensated by applying single qubit operators such as  $\sigma_z$ .

### 3.4. Identifying the gate parameters

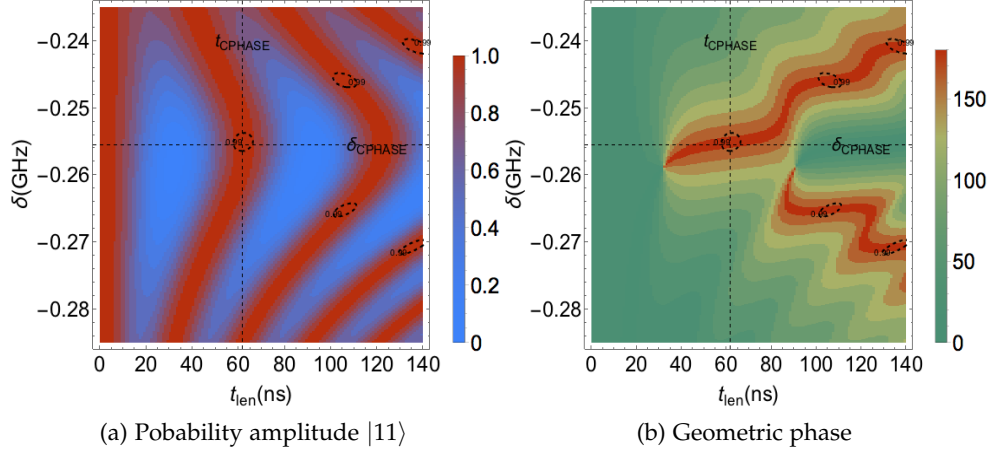


Figure 3.4: The intersection of two grid lines at  $t_{\text{CPHASE}}$  and  $\delta_{\text{CPHASE}}$  identify the optimal gate parameters.

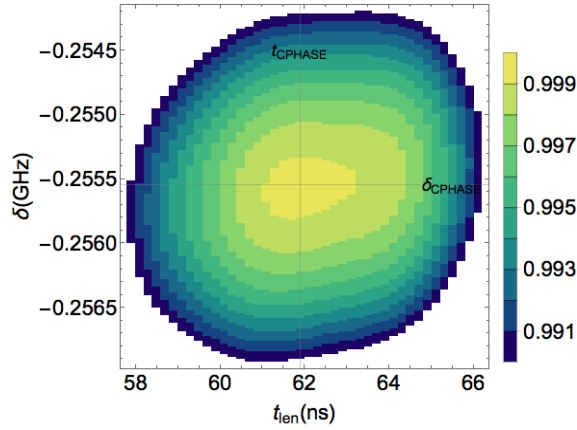


Figure 3.5: Simulated fidelity landscape for  $\hat{U}_{\text{sim}}$  operation. This shows the fastest parameter set resulting in CPHASE operation. The maxima occurs when most of the population is received back to  $|11\rangle$  subsystem while at the same time picking up geometric phase of -1.

### 3.5 Investigating the gate adiabaticity

Other values of adiabaticity parameters were also investigated. In addition to the configuration standard in the lab with  $\sigma=1.78$  ns, Figure 3.6 and Figure 3.7 shows population and geometric phase landscape for two more adiabaticity parameters, at 3.57 ns and 5.34 ns. Two contours on top of these landscapes are indicating fidelities of 99.8% and 99.9%. As can be observed, adiabaticity of gate in this range doesn't affect the maximal attainable fidelity. All three landscapes show that high fidelity over 99.9% is possible at all these adiabaticity parameters. This is a useful finding considering impracticality in attaining strong non-adiabatic regimes in the outputting of flux pulse. The AWG has a resolution of about 0.8 ns in time, and thus the sampling rate around the edges of flux pulse is limited by this resolution. Furthermore, it can be seen that as  $\sigma$  gets larger, more and more population is received back to the computational subsystem at the optimal gate parameters. But this comes at the cost of ever increasing gate execution time. Besides, maximum for population doesn't necessarily occur at the optimal gate parameters. The geometric phase of  $180^\circ$  is received at optimal gate parameters for all these adiabaticities. Again, the geometric phase landscape is tilted more and more with increasing adiabaticity parameter due to the fact that some conditional phase is picked by the qubits during the ever-increasing pulse rise time.

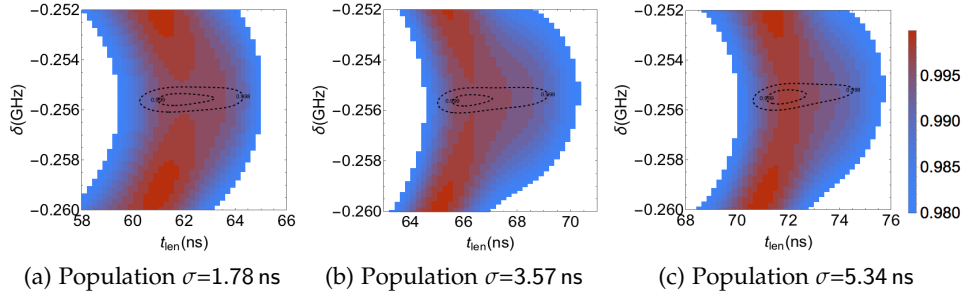


Figure 3.6: Population landscape of  $|11\rangle$  state for different adiabaticity parameters  $\sigma$ . Roughly 99.5% of population is received back to the sub-system. For all these adiabaticities, fidelities higher than 99.9% is attainable.

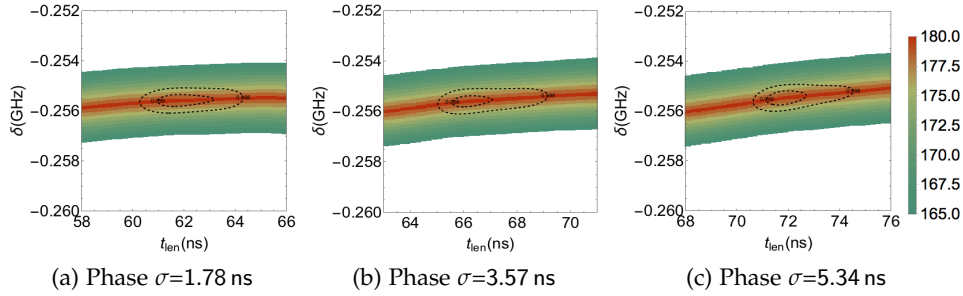


Figure 3.7: Geometric phase landscape for the two-qubit state for different adiabaticity parameters  $\sigma$ . Geometric phase of  $-1$  is achieved for all the investigated adiabaticities. The landscape looks increasingly tilted due to some conditional dynamic phases picked up during the gate time.

### 3.6 Experimental results

To compare the simulation results, the experiments in this thesis were performed with the help of setup shown in Figure 3.8. Four transmon type qubits can be seen in the setup. These qubits have lifetime on the order of few  $\mu s$ . Qubits are capacitively coupled to coplanar transmission line resonators for the purpose of readout. Due to the strong qubit-resonator coupling, the qubit-state-dependent resonator frequency shift is induced even when qubit frequency is far detuned from the resonator. The readout of the qubit state is performed in the dispersive-regime, as discussed in Section 2.2 (Wallraff et al., 2004). Because the transmitted signal is very weak, it is amplified using a quantum limited Josephson Parametric Dimer (JPD). Furthermore, voltage bias lines and flux lines can be seen for qubits in the sample. Flux lines are used to detune the qubits from their parking position. This is impor-

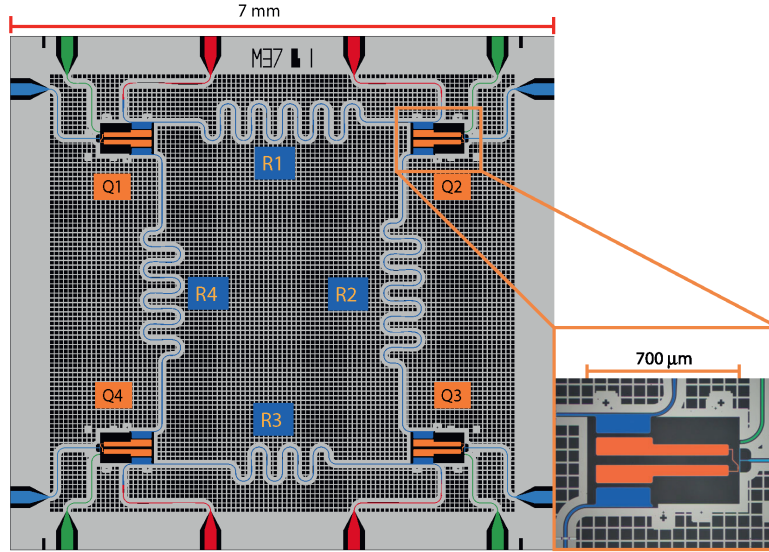


Figure 3.8: Four transmon-type qubit quantum processor are coupled to resonators R1 through R4. Red ports allow readout of the signals through resonators R1 and R3. The blue and green ports indicate flux biases and microwave drive lines. These ports are required to perform single and two-qubit operations (Salathe et al., 2015).

tant for two-qubit conditional gate implementation when sudden switching of interaction between qubits is needed.

Time-resolved measurement of signal transmitted through the resonator is required to perform the qubit readout. The noise present in the transmitted signal is further reduced by repeating the experiments several times. This transmitted signal can be decomposed into the so called in-phase  $I$  and quadrature  $Q$  components. These components depend non-linearly on the dispersive shift operator of resonator frequency, and is different for qubits in ground state or excited state. More details on the readout of qubits can be read from (Steffen, 2013) and (Baur, 2012).

To experimentally estimate the optimum pulse parameters to implement the CPHASE gate, the Chevron pattern is measured. At first, the qubits are excited to  $|11\rangle$  state using  $\pi$ -pulse. Then the flux pulse with varying amplitude and length is applied to one of the qubits to tune qubit A to qubit B. This gives the 2-D Chevron landscape as shown in Figure 3.9. At resonance, the population in  $|11\rangle$  state undergoes oscillation at the smallest frequency, given by  $J_0$  coupling. For pulse length near  $1/2J_0$ , at resonance, the population comes back to  $|11\rangle$  state picking up a geometric phase of  $-1$ . In addition, qubits also pick up some dynamic phases, and this is compensated by the short pulse seen at the beginning of the flux pulse in Figure 3.10.

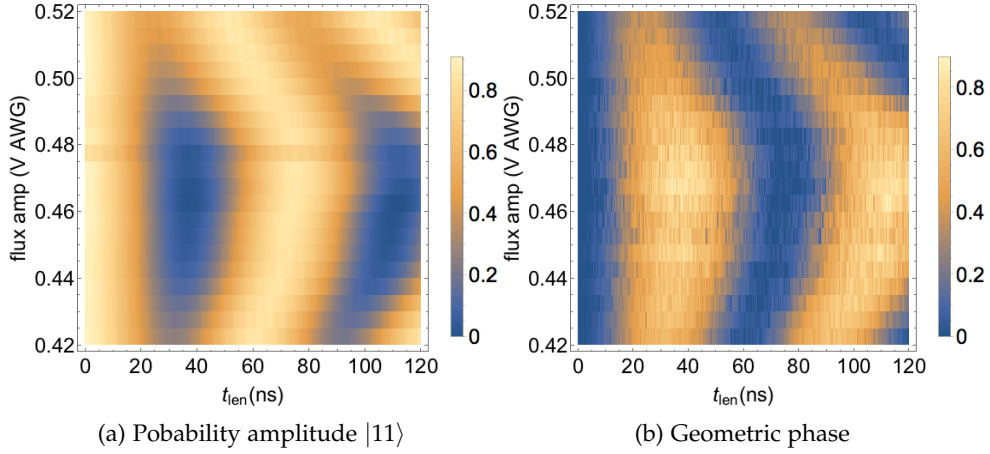


Figure 3.9: Experimental measurements demonstrating population oscillating between states  $|11\rangle$  and  $|20\rangle$ . As expected from the simulation, the Chevron pattern is asymmetric about the resonance..

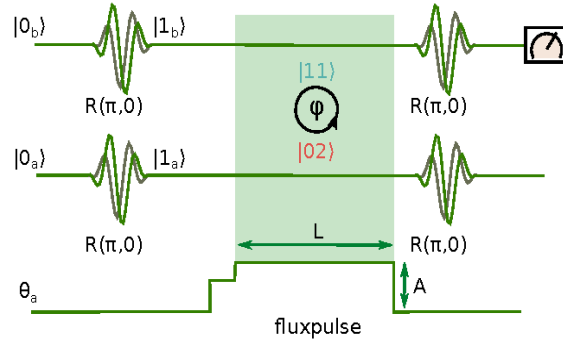


Figure 3.10: Pulse sequence for the experimental implementation of CPHASE gate. The flux pulse is used to tune  $|11\rangle$  and  $|20\rangle$  states to resonance, while  $\pi$ -pulses are applied to excite the qubits. (Heinsoo, 2013)

# Non-adiabatic error

---

The fact that flux pulse is suddenly switched on means the so-called non-adiabatic error will be present. Non-adiabatic error, in this thesis is loosely characterized as the amount of population that does not come back to the  $|11\rangle$  state during the gate time. This irreversible population leakage is observed because of the non-unitary evolution of the qubits system as the population is escaping into other qubits energy states (or degrees of freedom) which one has no control over. The probability of non-adiabatic population leakage into other higher level states of the qubits is given by the well-known Landau-Zener theory. More about Landau-Zener theory could be better understood from the article (Martinis and Geller, 2014). In Figure 4.1. the non-adiabatic error is more visible at smaller  $\sigma$  than the one investigated for the 2-dimensional landscapes above. Therefore, only  $\sigma$ 's below 0.2 ns was looked in this section.

As can be seen in the population leakage plot in Figure 4.1, the non-adiabatic error gets exponentially larger, as the adiabatic parameter  $\sigma$  gets smaller. In addition, as seen in Figure 4.2, Fidelity decreases as the pulse is switched on faster. To get these plots, 84 different  $\sigma$  were swept through. *FindMaximum* optimizer of *Wolfram Mathematica* was employed on the fidelity landscapes corresponding to each of the values of  $\sigma$ . The expression of fidelity in Equation 3.9 was taken, and the optimum pulse parameters that maximizes the fidelity was obtained. Because of the faster convergence rate, *NewtonMethod* was used as a method for the optimizer. For maximum accuracy, optimizer was provided with a guess value for  $\delta$  and  $t_{len}$ . The guess value for the next  $\sigma$  parameter was taken as the optimized value of the previous  $\sigma$ . The fidelity maximum was obtained for the simulated  $\sigma$  values. Hence, population leakage was calculated using the optimized results for  $\delta$  and  $t_{len}$  for all the adiabaticity parameters under investigation.



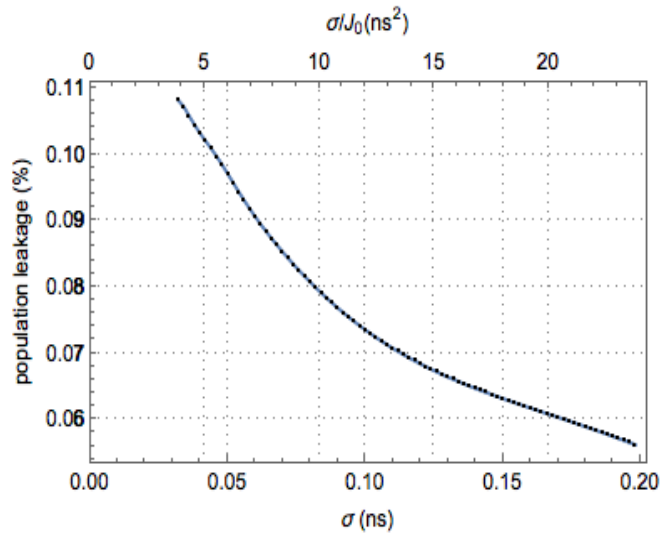


Figure 4.1: Population leakage increases exponentially as the pulse is switched on faster.

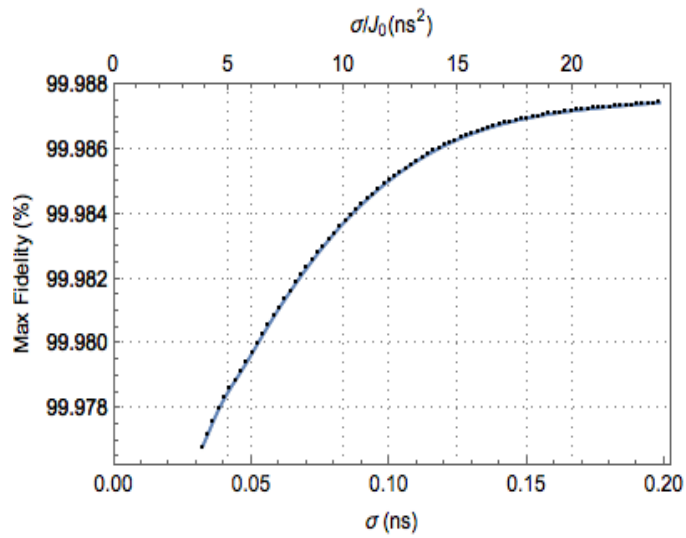


Figure 4.2: Maximum fidelity decreases exponentially with decreasing adiabaticity parameter. At  $\sigma=0.2$  ns fidelity as high as 99.99% can be achieved.

# Conclusion

---

In this thesis possibility of simulations of high fidelity CPHASE gate was shown in the regime between adiabatic and non-adiabatic limit. The Qudev lab CPHASE gate scheme uses adiabaticity parameter  $\sigma$  of 1.78 ns. At this parameter, gate fidelities above 99.9 % are attainable in the simulation. But it should be noticed that in the time-dependent hamiltonian other factors like  $T_1$  was not accounted. As infinite adiabaticity is impossible due to limited bandwidth of the signal generation electronics, the simulation of flux pulse is done by convoluting rectangular pulse with a Gaussian. Given the time dependent nature of Hamiltonian, numerical integration of Schrodinger equation was performed. To identify the exact parameters of the flux pulse in the implementation of the CPHASE gate, Chevron pattern was constructed for the probability amplitude of  $|11\rangle$  state. In addition, one also needs to look at the geometric phase landscape to have control over additional degree of freedom. For parameters used in lab, optimal gate pulse amplitude and length giving fidelity of 99.9 % were  $\delta = -0.255$  GHz and  $t_{len} = 61.9$  ns. Furthermore, strong non-adiabatic regime was also investigated. For  $\sigma$  below 0.2 ns non-adiabatic error was discovered. Meaning, less and less population was received back to the computational sub-system during the gate time below  $\sigma = 0.2$  ns. In this regime, sudden switching of the pulse leads to more population escaping into other states of the system.

## Acknowledgements

I would like to thank my supervisor, Johannes Heinsoo, for this semester project. He taught me many essential concepts of quantum information processing. Besides, his witty humor always enabled a positive atmosphere around me. In addition, I would like to thank Prof. Andreas Wallraff for giving me this chance to work in the group. The opportunity to get hands-on experience on cutting-edge quantum computing technology was priceless. I would also like to thank Michele Collodo and Markus Oppliger who helped me run my experiment when I was stuck in the absence of Johannes. I would also like to thank Sebastian Krinner for listening to my rehearsal presentation, and giving me feedback on it. At last but not the least, I am grateful for many interesting physics discussion with my former classmates, Brad Mitchell and Axel Dahlberg.

---

# Appendix

---

## A.1 Simulation results in non-adiabatic regime

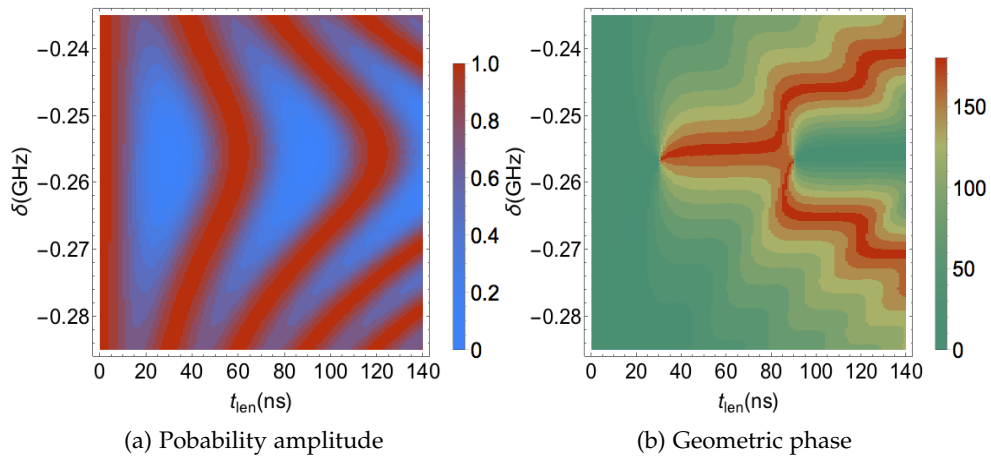


Figure A.1: The landscapes was created at  $\sigma = 0.05$  ns. This is to confirm the validity of the simulation results by comparison to the previous work (Heinsoo, 2013). At non-adiabatic regimes, both the population and geometric phase landscapes look increasingly symmetric about resonance  $\delta = -0.2555$  GHz.

## A.2 Wolfram Mathematica framework for simulations

The magnetic flux pulse was constructed by convoluting the square pulse with gaussian of certain standard deviation  $\sigma$ . Internal function of *Wolfram Mathematica* called *UnitBox* was used to model the rectangular pulse. The parameters that manipulates the shape of the pulse is also given under *fpulseparams*.

```

gaussian[\[Sigma]-] := PDF[NormalDistribution[0, \[Sigma]], t];
pulse = Simplify[
  Convolve[\[Delta] UnitBox[(t - offset)/(len)], gaussian[\[Sigma]],
    t, t2], Assumptions -> {len > 0}];
fpulseparams = {offset -> 52 + 3\[Sigma], \[Sigma] -> 1.78,
  t2 -> t};

```

Following function is implemented for computing the propagator numerically for the time-dependent hamiltonian  $h$ . Below *tfinal* represents the total simulation window and *n* represents the total number of iterations performed of Equation 3.8.

```

propagator[h-, tinit-, tfinal-, n-] :=
Module[{dt = N[(tfinal - tinit)/n],
  recuEq = IdentityMatrix[Length@h[0]]},
  Do[recuEq = MatrixExp[-I*h[t]*dt].recuEq, {t, tinit, tfinal - dt,
    dt}];
  recuEq]

```

Following function returns the probability amplitude of the  $|11\rangle$  state.

```

population[\[Delta]-, Subscript[t, len-]] :=
  Abs[Ket[11]\[Conjugate].(propagator[
    h[#, \[Delta], Subscript[t, len]] &, 0, 120, 600)].Ket[11]]^2;

```

---

## Bibliography

---

- Baur, M. (2012). *Realizing quantum gates and algorithms*. PhD thesis, ETH Zurich.
- Berry, M. (1984). "Quantal phase factors accompanying adiabatic changes". *Proc. R. Soc. Lond. A* 392, 45-57.
- Cottet, A. (2002). *Implementation of a quantum bit in a superconducting circuit*. PhD thesis, Universit Paris.
- Dahlberg, A. (2016). *Qubit state population from linearly independent system response*. Semester Thesis, ETH Zurich.
- Devoret, M. H. (1997). "Quantum fluctuations in electrical circuits". *Elsevier Science B.V.*
- Dewes, A. (2012). *Demonstrating quantum speedup with a two-transmon quantum processor*. PhD thesis, Universit Pierre et Marie Curie.
- Heinsoo, J. (2013). *Automatic multi-qubit gate calibration*. Semester Thesis, ETH Zurich.
- Koch, J., Yu, T. M., Gambetta, J., Houck, A. A., Schuster, D. I., Majer, J., Blais, A., Devoret, M. H., Girvin, S. M., and Schoelkopf, R. J. (2007). "Charge-insensitive qubit design derived from the cooper pair box". *Phys. Rev. A*, 76, 042319.
- Martinis, J. and Geller, M. (2014). "Fast adiabatic qubit gates using only  $\sigma_z$  control". *Phys. Rev. A*, 90, 0220307.
- Nakamura, Y., Chen, C. D., and Tsai, J. S. (1997). "Spectroscopy of energy-level splitting between two macroscopic quantum states of charge coherently superposed by josephson coupling". *Physical Review Letters*, 79, 2328-2331.

- Nielsen, M. A. and Chuang, I. L. (2000). *Quantum computation and quantum information*. Cambridge University Press, Cambridge ; New York, 1 edition.
- Pedersen, H. (2008). *Neutral atom quantum computing with Rydberg blockade*. PhD thesis, University of Aarhus.
- Salathe, Y., Mondal, M., Oppliger, M., Heinsoo, J., Kurpiers, P., Potocnik, A., Mezzacapo, A., Heras, U. L., Lamata, L., Solano, E., Filipp, S., and Wallraff, A. (2015). "Digital quantum simulation of spin models with circuit quantum electrodynamics". *Phys. Rev. X*, vol. 5, page 021027, 06 2015.
- Steffen, L. (2013). *Quantum teleportation and efficient process verification of superconducting circuits*. PhD thesis, ETH Zurich.
- Strauch, F. W., Johnson, P. R., Dragt, A. J., Lobb, C. J., Anderson, J. R., and Wellstood, F. C. (2003). "Quantum logic gates for coupled superconducting phase qubits". *Phys. Rev Lett.*, 91, 167005-(2003).
- Taylor, B. N., Parker, W. H., Langenberg, D. N., and Denenstein, A. (1967). "On the use of the ac josephson effect to maintain standards of electromotive force". *Metrologia*, 3(4):89.
- Tinkham, M. (1975). *Introduction to superconductivity*. McGraw-Hill International Editions, New York, 1 edition.
- Wallraff, A., Schuster, D. I., Blais, A., Frunzio, L., Huang, R.-S., Majer, J., Kumar, S., Girvin, S. M., and Schoelkopf, R. J. (2004). "Strong coupling of a single photon to a superconducting qubit using circuit quantum electrodynamics". *Nature*, 431, 162-167.



Eidgenössische Technische Hochschule Zürich  
Swiss Federal Institute of Technology Zurich

## Declaration of originality

The signed declaration of originality is a component of every semester paper, Bachelor's thesis, Master's thesis and any other degree paper undertaken during the course of studies, including the respective electronic versions.

Lecturers may also require a declaration of originality for other written papers compiled for their courses.

I hereby confirm that I am the sole author of the written work here enclosed and that I have compiled it in my own words. Parts excepted are corrections of form and content by the supervisor.

**Title of work** (in block letters):

SIMULATIONS OF CPHASE GATE ADIABATICITY

**Authored by** (in block letters):

*For papers written by groups the names of all authors are required.*

**Name(s):**

Thapa

**First name(s):**

Manish

With my signature I confirm that

- I have committed none of the forms of plagiarism described in the 'Citation etiquette' information sheet.
- I have documented all methods, data and processes truthfully.
- I have not manipulated any data.
- I have mentioned all persons who were significant facilitators of the work.

I am aware that the work may be screened electronically for plagiarism.

**Place, date**

Zurich, 13.03.16

**Signature(s)**

*For papers written by groups the names of all authors are required. Their signatures collectively guarantee the entire content of the written paper.*